Journal of Dental Sciences 19 (2024) 837–845

Available online at www.sciencedirect.com

ScienceDirect

journal homepage: www.e-jds.com

Original Article

3D finite element analysis of stress distribution on the shape of resected root-end or with/without bone graft of a maxillary premolar during endodontic microsurgery

Aein Mon [a], Mi-El Kim [b], Kee-Yeon Kum [c**], Ho-Beom Kwon [a*]

[a] *Dental Research Institute and Department of Prosthodontics, School of Dentistry, Seoul National University, Seoul, Republic of Korea*
[b] *Dental Research Institute and Department of Oral Anatomy, School of Dentistry, Seoul National University, Seoul, Republic of Korea*
[c] *Dental Research Institute and Department of Conservative Dentistry, School of Dentistry, Seoul National University, Seoul, Republic of Korea*

Received 17 July 2023; Final revision received 29 August 2023
Available online 16 September 2023

KEYWORDS
Apical stress;
Apicoectomy;
Finite element analysis;
Round resection;
Targeted endodontic microsurgery

Abstract *Background/purpose:* Apical root resection pattern affects the stress distribution behavior in the apical region of the resected tooth. The purpose of the study was to compare the biomechanical responses of resected teeth between endodontic microsurgery (horizontal resection) and targeted endodontic microsurgery (round resection).
Materials and methods: Five different models were developed. The basic model without resection (NR) was regarded as the control model, and the others involved: horizontal resection without bone grafting (HN), horizontal resection with bone grafting (HG), round resection without bone grafting (RN), and round resection with bone grafting (RG) models. A static load of 100 N was applied to the buccal and palatal cusps of all the teeth in a 30° oblique direction. The maximum von-Mises stress and tooth displacement values were analyzed and compared.
Results: Both the HN and RN models exhibited lower stress distribution values on bone compared with the NR (control) model. Regarding maximum stress distribution at the root apex, the stress value of the RN model was slightly higher compared to the HN model, whereas the RG model displayed a slightly lower stress value in comparison with the HG model. For

* Corresponding author. Dental Research Institute and Department of Prosthodontics, School of Dentistry, Seoul National University, 101, Daehak-ro, Jongno-gu, Seoul 03080, Republic of Korea.
** Corresponding author. Dental Research Institute and Department of Conservative Dentistry, School of Dentistry, Seoul National University, 101, Daehak-ro, Jongno-gu, Seoul 03080, Republic of Korea.
E-mail addresses: kum6139@snu.ac.kr (K.-Y. Kum), proskwon@snu.ac.kr (H.-B. Kwon).

https://doi.org/10.1016/j.jds.2023.08.029

maximum tooth displacement value, there were no significant differences between the HN and RN models, as well as the HG and RG models.
Conclusion: The round resection pattern had comparable stress distribution behaviors at the root apex and tooth displacement values with the horizontal resection pattern. Targeted endodontic microsurgery might provide better biomechanical response of the resected tooth after root-end resection.

Introduction

Apical root resection is a biologically important procedure in endodontic microsurgery where an infected or damaged portion of the apical 3 mm of the root is surgically removed.[1,2] It is typically indicated when the tooth condition is beyond conventional endodontic salvageability[3–5] or sometimes, there is a periapical lesion or cyst present that is essential to be removed surgically and to diagnose histologically.[6]

A root-end surgical procedure involves the exposure of the apical region of the infected tooth through an osteotomy and removing the apical portion of the tooth perpendicular to the root axis.[7] This surgical protocol has some difficulties in locating the precise entry point on the bone surface during the osteotomy, and the entire procedure relies on mental navigation based on a cone-beam computed tomography (CBCT) image. Therefore, using such a surgical approach has some drawbacks, such as a significant amount of bone loss due to the large osteotomy size and unintentional damage to important vital structures.[4] Moreover, it can cause apical or coronal deviations during root-end resection, which can consequently lead to suboptimal results and complications.

Precision is crucial in the performance of root-end surgery. With diverse applications of digital workflows in dentistry, targeted endodontic microsurgery is currently trending for its minimal invasiveness and promising results.[8–14] A 3-dimensional (3D)-printed surgical stent directs the trephine bur during the osteotomy and root-end recession in targeted endodontic microsurgery. Implant planning software and the CBCT image are utilized for digital planning, where the custom implant features are used to determine the dimensions of the stent tube.[15,16] Recently, digital models of custom trephine burs have been incorporated into the existing implant software.[17]

There are some concerns about apical root resection. The pattern of apical root resection has a big impact on the stress distribution behavior in the apical region of the resected tooth. Previous studies reported that it is preferable to perform perpendicular cutting to the long axis of the tooth with consideration of biological and biomechanical outcomes.[18,19] However, using a trephine bur as a part of targeted endodontic microsurgery leaves a round resection pattern at the apex of the tooth, despite being digitally planned in a perpendicular direction to the long axis of the tooth. According to a photoelastometric study conducted by Sauveur et al.,[20] a resection pattern that leaves a peculiar angle in the apical area was related to the density of fringes focused on the lingual edge of the apical portion of the tooth, reflecting mechanical stresses. Therefore, the pattern of the remaining root apex after root-end resection is critical in evaluating how this resection pattern influences the biomechanical outcomes of the resected teeth prior to surgical treatment.

Finite element analysis (FEA) has been commonly employed in the field of dentistry as a non-invasive and powerful tool to analyze the biomechanical responses of complex intraoral structures.[21–24] FEA method is basically the discretization of a complex structure into smaller, more manageable elements, which are then mathematically modeled using equations and numerical methods. By solving these equations, it can predict the response of the structure to a certain force or load, contributing information about stress distribution, strain patterns, and potential areas of weakness in the structure. Such comprehensive information about stress and strain is difficult to achieve through alternative experimental or analytical means due to the intricate and delicate nature of intraoral structures as well as the complex interactions of various forces and loads within this confined environment.

The purpose of this FEA study was to compare the biomechanical responses of the resected tooth between endodontic microsurgery (horizontal resection) and targeted endodontic microsurgery (round resection).

Materials and methods

Basic 3D geometric model development

The CBCT data of a female patient aged 52 was used for this FEA study with informed consent, and the study was approved by the institutional review board (CRI12016). A 3D geometric model of the maxillary bone segment, including the teeth from the first premolar to the second molar, was developed based on the patient's CBCT data using Mimics software (Version 19.0; Materialise NV, Leuven, Belgium). The maxillary second premolar was the tooth requiring a root-end surgery, and the maxillary first molar was the implant. The geometry of this external hex implant (Osstem Implant, Seoul, Korea) was obtained from the manufacturer. The alveolar bone crest was 1 mm below the cementoenamel junction of the teeth. The periodontal ligament was simulated with a thickness of 200 μm.[25] This basic model without resection (NR) was regarded as the control model (Fig. 1A).

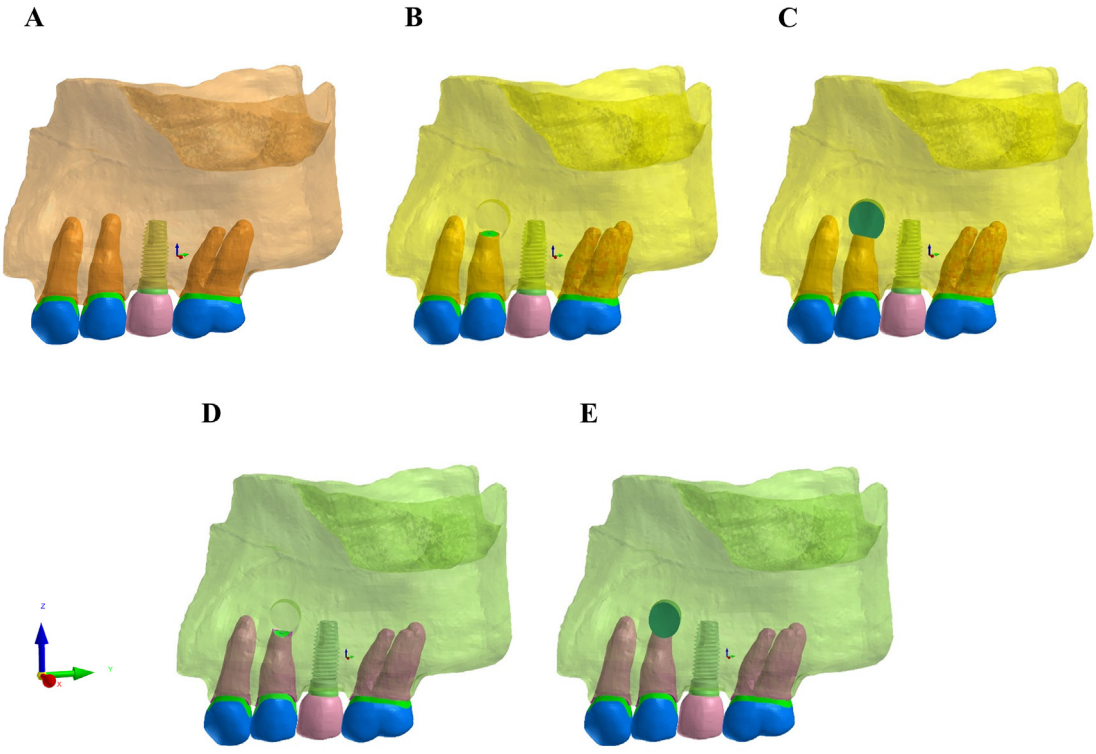

Figure 1 Views of the five different models: (A) NR model (no resection, control); (B) HN model (horizontal resection without bone grafting); (C) HG model (horizontal resection with bone grafting); (D) RN model (round resection without bone grafting); and (E) RG model (round resection with bone grafting).

Table 1 Description of the models.

Model	Resection pattern	Description
NR	No resection (control)	Basic model
HN	Horizontal resection without bone grafting	5 mm osteotomy, 3 mm apical resection, 3 mm MTA[a] retro filling, no bone grafting
HG	Horizontal resection with bone grafting	5 mm osteotomy, 3 mm apical resection, 3 mm MTA retro filling, bone grafting
RN	Round resection without bone grafting	4.5 mm osteotomy, 3 mm apical resection, 3 mm MTA retro filling, no bone grafting
RG	Round resection with bone grafting	4.5 mm osteotomy, 3 mm apical resection, 3 mm MTA retro filling, bone grafting

[a] MTA: mineral trioxide aggregate.

Table 2 Number of nodes and elements.

Model	Nodes	Elements
NR[a]	156,112	812,546
HN[b]	164,940	842,188
HG[c]	165,827	849,001
RN[d]	161,119	843,626
RG[e]	161,812	849,212

[a] NR: no resection.
[b] HN: horizontal resection without bone grafting.
[c] HG: horizontal resection with bone grafting.
[d] RN: round resection without bone grafting.
[e] RG: round resection with bone grafting.

Table 3 Material Properties.

Material	Elastic modulus (GPa[a])	Poisson's ratio
Cancellous bone	1.37	0.30
Enamel	41	0.30
Dentin	18.6	0.31
Pulp	0.00207	0.45
PDL[b]	0.05	0.49
Gutta-percha	0.00069	0.45
Composite resin	12	0.33
MTA[c]	22.4	0.25
Bio-Oss	15	0.30
Titanium	102	0.30
Gold	100	0.30

[a] GPa: gigapascal.
[b] PDL: periodontal ligament.
[c] MTA: mineral trioxide aggregate.

Generation of 3D finite element models

Another four different models were developed following the type of resection on the biomechanical response of the resected tooth, with the simulation of endodontic microsurgery and targeted endodontic microsurgery (Fig. 1B—E). The detailed descriptions of the models are shown in Table 1. Root canal treatments, gutta-percha obturations, and resin core restorations were simulated based on the NR model.

For the simulation with endodontic microsurgery (horizontal resection), a 5 mm diameter osteotomy and 3 mm root-end resection, which was perpendicular to the long axis of the tooth, were performed. A horizontal resection pattern was conducted at the apical 3 mm of the root to reproduce conventional cutting with a bur. Afterward, a 3 mm retro filling with MTA was virtually conducted in the surgically treated model. With this horizontal resection, two different models were developed: one was "the horizontal resection without bone grafting" (HN) (Fig. 1B) and the other was "the horizontal resection with bone grafting" (HG) (Fig. 1C).

Osteotomies and root-end resections using a 4.5 mm diameter trephine bur were meant to be performed perpendicular to the long axis of the tooth for the simulation with targeted endodontic microsurgery (round resection). A round resection pattern was conducted at the apical 3 mm of the root to reflect guided surgery with a trephine bur. Subsequently, a 3 mm root-end filling with MTA was virtually conducted in the surgically treated model. With this round resection, two different models were created: one was "the round resection without bone grafting" (RN) (Fig. 1D), and the other one was "the round resection with bone grafting" (RG) (Fig. 1E).

Meshing and material properties

Tetrahedral meshes of all the components in each model were generated for FEA using the Visual-Mesh program (Version 16.5, ESI Group, Paris, France). Configurations of the models, including the number of nodes and elements, are shown in Table 2. The material properties of all the components used in this FEA study were based on previous

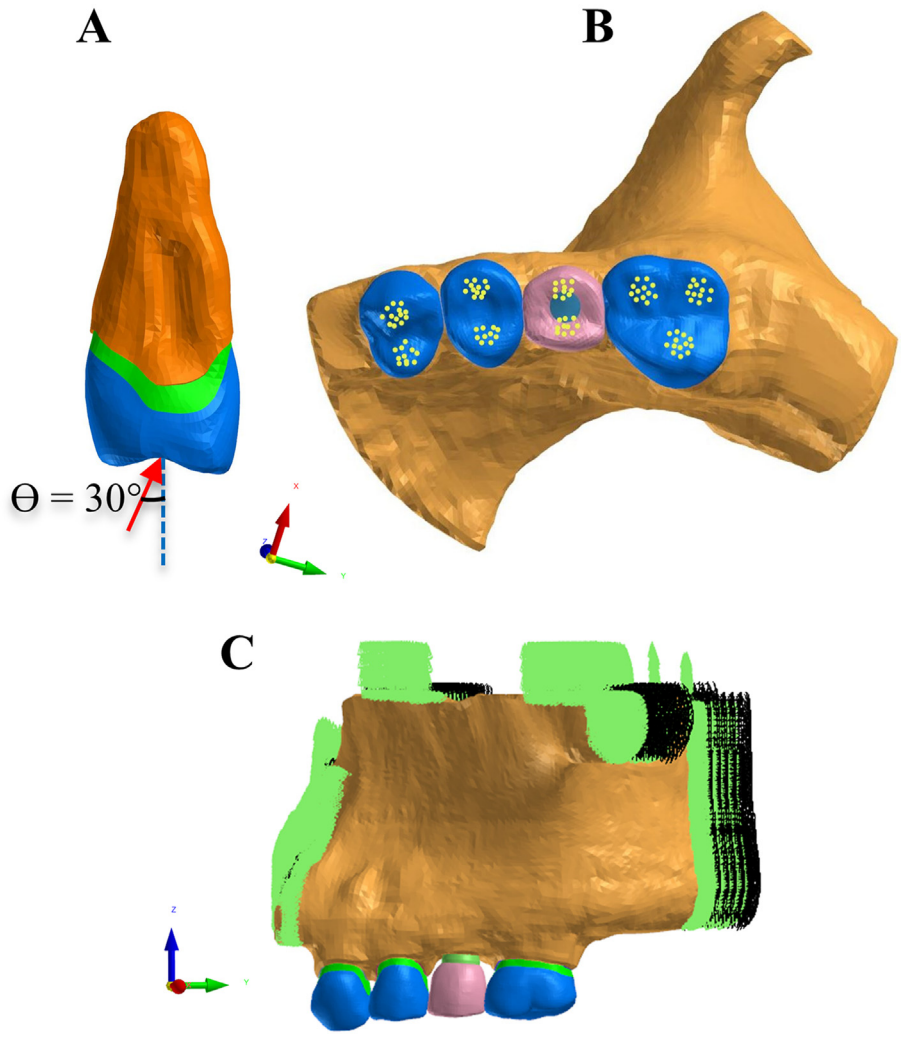

Figure 2 Loading and boundary conditions: (A) Mesial view, direction of the applied force; (B) occlusal view, force acting points distributed on the triangular ridges of the buccal and palatal cusps of the teeth; (C) boundary constraints at the cutting surface of the maxillary bone.

studies[22,24,26–31] are summarized in Table 3, and were assumed to be homogenous, isotropic, and linearly elastic. Moreover, all components within the models were assumed to be perfectly attached or connected to each other, without any separation or relative movement allowed between the components.

Boundary constraints and loading condition

As boundary conditions, all the nodes of the cutting surface of the maxillary bone were restricted in all directions. The masticatory forces that are generated during the process of chewing and grinding food are not purely vertical and occur at certain angulations. In accordance with a human clinical experimental study, the typical force exerted during the chewing motion ranges from 20 to 120 N.[32,33] Therefore, in this study, a static load of 100 N was applied to the triangular ridges of the buccal and palatal cusps of all teeth in a 30° oblique direction to stimulate masticatory forces (Fig. 2A and B). The analysis was processed using the Visual-Crash software (Version 16.5, ESI Group). The maximum von-Mises stress and tooth displacement values were analyzed and compared for each component of all the models.

Results

Table 4 shows the maximum von-Mises stress values of different components of each model.

Stress distribution on the bone

The maximum von-Mises stress on the bone was higher for the RN model compared to the HN model. However, in comparison with the NR (control) model, both the HN and RN models exhibited lower stress distribution values on the bone. Using bone grafting, the maximum von-Mises stress on the bone decreased to 77% in the RG model, whereas there was no obvious alteration in the HG model (Fig. 3A).

Table 4 Maximum von-Mises stress values (MPa[a]) of different components of each model.

Model	NR[b]	HN[c]	HG[d]	RN[e]	RG[f]
Bone	10.9	5.2	5.1	10	7.7
Dentin	8.2	4	11.4	5.3	10.8
Enamel	10.9	12.4	15.3	11.8	13
PDL[g]	0.5	0.5	0.5	0.6	0.6
Gutta-percha	-	0.004	0.006	0.005	0.007
MTA[h]	-	2	3.2	2.6	4
Resin	-	7.3	9.3	8.8	8.2
Bone graft	-	-	8.4	-	8.1

[a] MPa: megapascal.
[b] NR: no resection.
[c] HN: horizontal resection without bone grafting.
[d] HG: horizontal resection with bone grafting.
[e] RN: round resection without bone grafting.
[f] RG: round resection with bone grafting.
[g] PDL: periodontal ligament.
[h] MTA: mineral trioxide aggregate.

Stress distribution at the root apex

Regarding maximum stress distribution at the root apex, both the HN and RN models exhibited a lower stress distribution value compared with the control model, where the maximum stress value of the RN model was slightly higher compared to the HN model. However, in the comparison between the HG and RG models, the maximum stress concentration at the root apex of the RG model was slightly lower than the HG model (Figs. 3B and 4).

Displacement distribution

For the maximum tooth displacement value of the resected tooth, there were no significant differences between the HN and RN models, as well as the HG and RG models. Moreover, all the HN, HG, RN, and RG models exhibited almost the same tooth displacement value as the control model (Fig. 5). There was a similar displacement

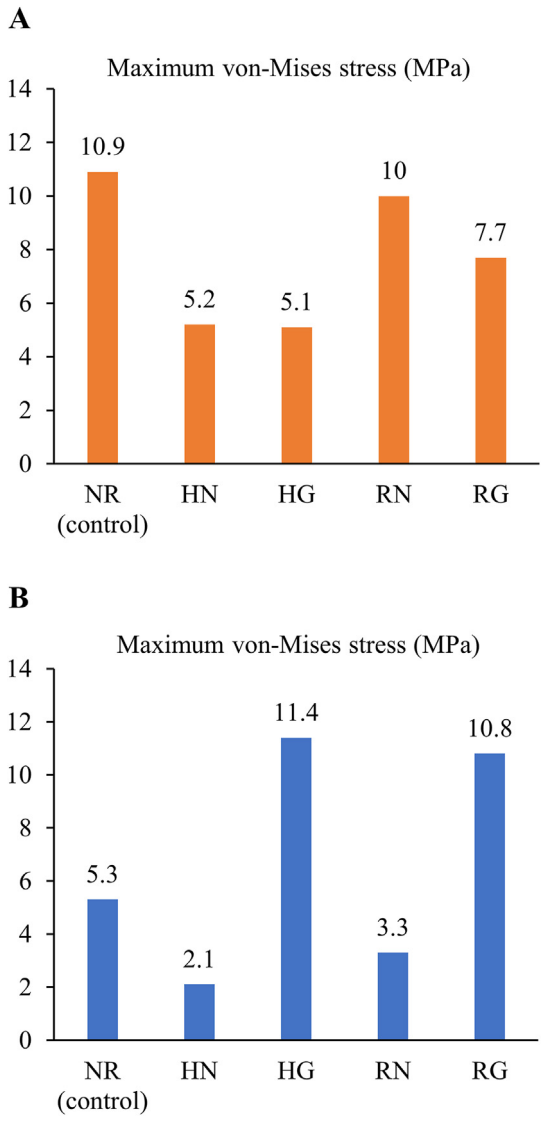

Figure 3 Maximum von-Mises stress values for each different model: (A) On the bone; (B) at the root apex.

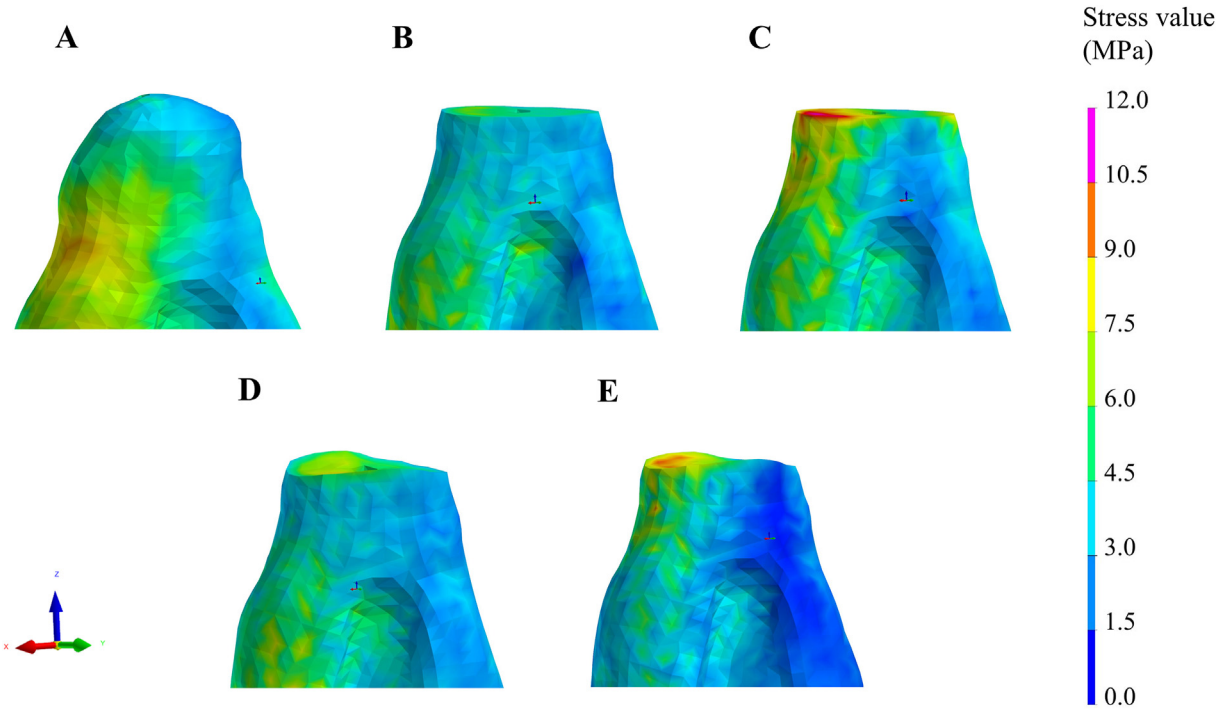

Figure 4 Stress distribution pattern at the root apex: (A) NR model (no resection, control); (B) HN model (horizontal resection without bone grafting); (C) HG model (horizontal resection with bone grafting); (D) RN model (round resection without bone grafting); and (E) RG model (round resection with bone grafting).

distribution pattern between the control and RG models, and displacement distribution patterns for each model are shown in Fig. 6.

Discussion

In a recent retrospective study assessing the clinical outcomes of 24 cases, it was reported that targeted endodontic microsurgery had a 91.7% success rate in a short-term assessment of 1 year.[34] However, long-term investigations that reveal the prognosis of targeted endodontic microsurgery are still needed. To ensure long-term prognosis, it is crucial to consider not only the biological aspects but also the biomechanical aspects of endodontic microsurgery. Therefore, maximum von-Mises stress and tooth displacement values of targeted endodontic microsurgery were analyzed through a finite element study before the findings of long-term follow-up studies.

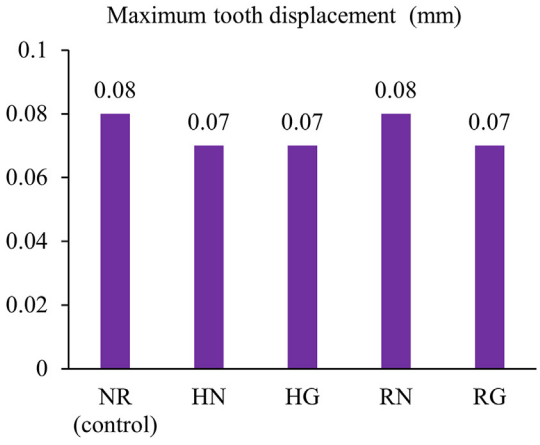

Figure 5 Maximum tooth displacement values for the resected tooth in each different model.

This study simulated two surgical conditions: endodontic microsurgery, which produces a horizontal resection pattern, and targeted endodontic microsurgery, which generates a round resection pattern. As a result, these different surgical situations had a minor impact on the biomechanical responses of the resected tooth.

Concerning the maximum von-Mises stress on the bone, the horizontal resection pattern following endodontic microsurgery exhibited a lower stress value compared with the round resection pattern that resulted from targeted endodontic microsurgery. The reason could be that exactly 90° of horizontal cutting perpendicular to the root axis was simulated in endodontic microsurgery. However, in clinical situations, it is sometimes impossible to obtain an accurate 90° angulation of the horizontal cut using a bur. On the other hand, targeted endodontic microsurgery provides precise perpendicular cutting with the aid of a digitally planned surgical guide.[16,35,36] Moreover, in a study comparing a surgical simulation between endodontic microsurgery and targeted endodontic surgery conducted by Hawkins et al.,[10] it was reported that targeted endodontic microsurgery provides a bevel angle more closely approaching zero degrees. In this study, it was observed that the maximum stress value of targeted endodontic microsurgery was lower than the control model, indicating an acceptable stress distribution on the bone. Moreover, bone grafting demonstrated greater favorable stress

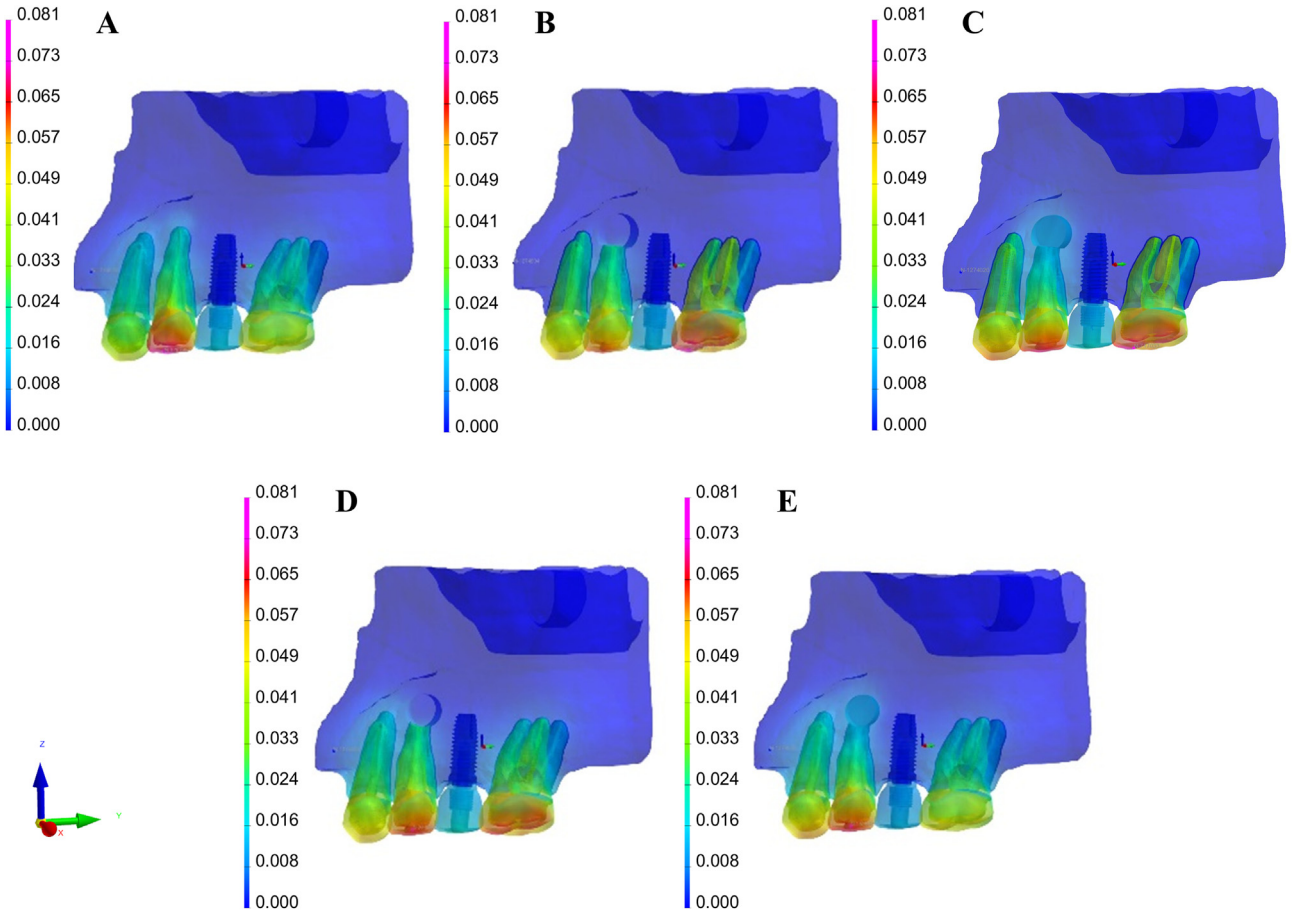

Figure 6 Tooth displacement distribution pattern following the type of resection: (A) NR model (no resection, control); (B) HN model (horizontal resection without bone grafting); (C) HG model (horizontal resection with bone grafting); (D) RN model (round resection without bone grafting); and (E) RG model (round resection with bone grafting).

distribution on the alveolar bone, which means the stresses exerted on the bone are more evenly dispersed and do not concentrate excessively in any particular area. Therefore, bone grafting is expected to contribute to the long-term success and stability of the treated tooth.

The pattern of the remaining root apex following root-end resection influences the biomechanical response of the resected tooth.[20] Therefore, in this study, we compared the stress distribution behaviors at the root apex between the horizontal and round resection patterns following two different surgical techniques. The results of the study showed that both patterns of resection induced lower stress distribution at the root apex compared to the control model. Although using a trephine bur to perform an apical resection resulted in a round resection pattern in the apical region of the resected tooth, the maximum stress value did not significantly differ from that obtained with a horizontal resection. The reason for this finding could be that both types of resections were conducted in a perpendicular plane. This behavior was also observed in previous studies where cutting in a perpendicular plane to the long axis of the tooth was related to positive biomechanical outcomes.[18–20]

Interestingly, using bone grafting, the maximum von-Mises stresses at the root apex were significantly increased in both patterns of resection, where round resection presented with a slightly more favorable outcome compared with horizontal resection. However, no bone resorption was suggested with both studied conditions as the micro-strain values were within the physiologic limit.[37]

Another important factor associated with the long-term prognosis of the endodontic surgery is the occurrence of clinical tooth mobility following apical root resection. Perlitsh[38] reported the capacity of the remaining attachment apparatus to reverse existing clinical tooth mobility, determined by the amount of remaining alveolar bone support. Therefore, in this study, maximum tooth displacement values were also analyzed to reproduce clinical tooth mobility. As a result, both horizontal and round resection patterns following respective surgical protocols exhibited similar displacement values in comparison with the control model. The explanation for this finding could be the remaining sufficient amount of residual supporting alveolar bone in both surgical settings.

von Arx et al.[39] stated the association between the diameter of bony defects in the periapical region and the clinical outcomes of endodontic surgery. Furthermore, in one prospective study regarding the clinical outcomes of endodontic microsurgery, it was reported that a positive clinical outcome can be expected with a residual of more than 3 mm of buccal bone height following the osteotomy.[40] The findings of this FEA study indicated the ability of the

remaining supporting tissue in preventing future clinical tooth mobility, supporting those previous findings.

In this FEA study, all the structures involved in the analysis were considered to be homogenous, isotropic, and linear. Moreover, the simulation of different structures, including tooth morphology, periodontal conditions, and endodontic procedures, could not exactly reflect real clinical situations. In this study, although the analysis was performed only with oblique occlusal loading, further studies with horizontal or vertical loadings are necessary to predict the biomechanical response of the resected tooth after targeted endodontic microsurgery.

Based on the findings of this study, the round resection pattern had comparable stress distribution behaviors at the root apex and tooth displacement values with the horizontal resection pattern. Therefore, within the limitations of this FEA study, it can be concluded that targeted endodontic microsurgery might provide better biomechanical response of the resected tooth after root-end resection.

Declaration of competing interest

The authors have no conflicts of interest relevant to this article.

Acknowledgments

This work was supported by the National Research Foundation of Korea (NRF) grant funded by the Korean government (MSIT) (No. 2021R1F1A1063506).

References

1. Gilheany PA, Figdor D, Tyas MJ. Apical dentin permeability and microleakage associated with root end resection and retrograde filling. *J Endod* 1994;20:22—6.
2. Pop I. Oral surgery: part 2. endodontic surgery. *Br Dent J* 2013;215:279—86.
3. Karabucak B, Setzer F. Criteria for the ideal treatment option for failed endodontics: surgical or nonsurgical? *Comp Cont Educ Dent* 2007;28:391—8.
4. Kim S, Kratchman S. Modern endodontic surgery concepts and practice: a review. *J Endod* 2006;32:601—23.
5. Lieblich SE. Endodontic surgery. *Dent Clin* 2012;56:121—32.
6. Nikitakis NG, Brooks JK, Melakopoulos I, et al. Lateral periodontal cysts arising in periapical sites: a report of two cases. *J Endod* 2010;36:1707—11.
7. Locurcio LL, Leeson R. A case of periradicular surgery: apicoectomy and obturation of the apex, a bold act. *Stomatological Dis Sci* 2017;1:76—80.
8. Ackerman S, Aguilera FC, Buie JM, et al. Accuracy of 3-dimensional-printed endodontic surgical guide: a human cadaver study. *J Endod* 2019;45:615—8.
9. Benjamin G, Ather A, Beuno MR, Estrela C, Diogenes A. Preserving the neurovascular bundle in targeted endodontic microsurgery: a case series. *J Endod* 2021;47:509—19.
10. Hawkins TK, Wealleans JA, Pratt AM, Ray JJ. Targeted endodontic microsurgery and endodontic microsurgery: a surgical simulation comparison. *Int Endod J* 2020;53:715—22.
11. Kim JE, Shim JS, Shin YS. A new minimally invasive guided endodontic microsurgery by cone beam computed tomography and 3-dimensional printing technology. *Restor Dent Endod* 2019;44:e29.
12. Peng L, Zhao J, Wang ZH, Sun YC, Liang YH. Accuracy of root-end resection using a digital guide in endodontic surgery: an in vitro study. *J Dent Sci* 2021;16:45—50.
13. Ray JJ, Giacomino CM, Wealleans JA, Sheridan RR. Targeted endodontic microsurgery: digital workflow options. *J Endod* 2020;46:863—71.
14. Smith BG, Pratt AM, Andreson JA, Ray JJ. Targeted endodontic microsurgery: implications of the greater palatine artery. *J Endod* 2021;47:19—27.
15. Ahn SY, Kim NH, Kim S, Karabucak B, Kim E. Computer-aided design/computer-aided manufacturing-guided endodontic surgery: guided osteotomy and apex localization in a mandibular molar with a thick buccal bone plate. *J Endod* 2018;44:665—70.
16. Tavares WLF, Fonseca FO, Maia LM, et al. 3D apicoectomy guidance: optimizing access for apicoectomies. *J Oral Maxillofac Surg* 2020;78:357. e1—8.
17. Antal M, Nagy E, Sanyo L, Braunitzer G. Digitally planned root end surgery with static guide and custom trephine burs: a case report. *Int J Med Robot Comput Assist Surg* 2020;16:e2115.
18. Gagliani M, Taschieri S, Molinari R. Ultrasonic root-end preparation: influence of cutting angle on the apical seal. *J Endod* 1998;24:726—30.
19. Monteiro JB, de Oliveira Dal Piva AM, Mendes Tribst JP, Souto Borges AL, Tango RN. The effect of resection angle on stress distribution after root-end surgery. *Iran Endod J* 2018;13:188—94.
20. Sauveur G, Boccara E, Colon P, Sobel M, Boucher Y. A photoelastimetric analysis of stress induced by root-end resection. *J Endod* 1998;24:740—3.
21. Geng JP, Tan KB, Liu GR. Application of finite element analysis in implant dentistry: a review of the literature. *J Prosthet Dent* 2001;85:585—98.
22. Chang HS, Chen YC, Hsieh YD, Hsu ML. Stress distribution of two commercial dental implant systems: a three-dimensional finite element analysis. *J Dent Sci* 2013;8:261—71.
23. Murakami N, Wakabayashi N. Finite element contact analysis as a critical technique in dental biomechanics: a review. *J Prosthodont Res* 2014;58:92—101.
24. Jang Y, Hong HT, Roh BD, Chun HJ. Influence of apical root resection on the biomechanical response of a single-rooted tooth: a 3-dimensional finite element analysis. *J Endod* 2014;40:1489—93.
25. Hohmann A, Kober C, Young P, et al. Influence of different modeling strategies for the periodontal ligament on finite element simulation results. *Am J Orthod Dentofacial Orthop* 2011;139:775—83.
26. Haecker CJ, Garboczi EJ, Bullard JW, et al. Modeling the linear elastic properties of Portland cement paste. *Cement Concr Res* 2005;35:1948—60.
27. Lanza A, Aversa R, Rengo S, Apicella D, Apicella A. 3D FEA of cemented steel, glass and carbon posts in a maxillary incisor. *Dent Mater* 2005;21:709—15.
28. Razaghi R, Mallakzadeh M, Haghpanahi M. Dynamic simulation and finite element analysis of the maxillary bone injury around dental implant during chewing different food. *Biomed Eng Appl Basis Commun* 2016;28:1650014.
29. Rees JS, Jacobsen PH. Elastic modulus of the periodontal ligament. *Biomaterials* 1997;18:995—9.
30. Rubin C, Krishnamurthy N, Capilouto E, Yi H. Stress analysis of the human tooth using a three-dimensional finite element model. *J Dent Res* 1983;62:82—6.
31. Zhang X, Tiainen H, Haugen HJ. Comparison of titanium dioxide scaffold with commercial bone graft materials through micro-finite element modelling in flow perfusion. *Med Biol Eng Comput* 2019;57:311—24.
32. Schindler HJ, Stengel E, Spiess WE. Feedback control during mastication of solid food textures— a clinical-experimental study. *J Prosthet Dent* 1998;80:330—6.

33. Ordinola-Zapata R, Lin F, Nagarkar S, Perdigão J. A critical analysis of research methods and experimental models to study the load capacity and clinical behaviour of the root filled teeth. *Int Endod J* 2022;55:471—94.
34. Buniag AG, Pratt AM, Ray JJ. Targeted endodontic microsurgery: a retrospective outcomes assessment of 24 cases. *J Endod* 2021;47:762—9.
35. Antal M, Nagy E, Braunitzer G, Frater M, Piffko J. Accuracy and clinical safety of guided root end resection with a trephine: a case series. *Head Face Med* 2019;15:1—8.
36. Popowicz W, Aleksandra, Ulatowska P, Kohli MR. Targeted endodontic microsurgery: computed tomography—based guided stent approach with platelet-rich fibrin graft: a report of 2 cases. *J Endod* 2019;45:1535—42.
37. Frost HM. Bone "mass" and the "mechanostat": a proposal. *Anat Rec* 1987;219:1—9.
38. Perlitsh MJ. A systematic approach to the interpretation of tooth mobility and its clinical implications. *Dent Clin* 1980;24:177—93.
39. von Arx T, Jensen SS, Hanni S, Friedman S. Five-year longitudinal assessment of the prognosis of apical microsurgery. *J Endod* 2012;38:570—9.
40. Song M, Kim SG, Shin SJ, Kim HC, Kim E. The influence of bone tissue deficiency on the outcome of endodontic microsurgery: a prospective study. *J Endod* 2013;39:1341—5.